Reprint from:

The South Atlantic

Present and Past Circulation

Edited by Gerold Wefer, Wolfgang H. Berger,
Gerold Siedler, David J. Webb

ISBN 3-540-62079-6

Mass and Heat Transports in the South Atlantic Derived from Historical Hydrographic Data

R. Schlitzer

Alfred-Wegener-Institute for Polar and Marine Research, Bremerhaven, GERMANY

Abstract: Mass and heat transports in the South Atlantic as well as exchange flows with the South Pacific and the Indian Ocean are determined by driving a conservative, steady box-model towards the historical temperature (θ) and salinity (s) observations. The optimal model circulation searched for is required (a) to approximately preserve the vertical velocity shear as given by geostrophic calculations and (b) to correctly reproduce the measured distributions of θ and s. Information contained in the θ/s data on baroclinic flows is exploited through constraint (a) and the unknown reference velocities are determined by the model in a way such that the resulting absolute flow velocities produce realistic θ and s fields (constraint (b)). The model is mass, heat and salt conserving and has realistic topography. The adjoint method is applied as an efficient means for calculating cost function gradients needed during the optimization process.
Model experiments show that indeed realistic θ and s model distributions can be obtained with flows that are consistent with geostrophy. Moreover, close agreement between measurements and model is obtained for a variety of model velocity fields that differ considerably with respect to strength of the meridional overturning cell and magnitude of meridional heat transports. The maximal acceptable meridional heat transport across 30°S (based on an evaluation of θ/s misfits and deviations from geostrophic shear) amounts to 0.4 PW. Forcing the model to produce larger heat fluxes results in systematic property misfits in the upper layers of the South Atlantic. Contrary to most published heat transport estimates the model also accommodates poleward (southward) heat fluxes of up to -0.5 PW. The best model property fields are obtained for a heat transport across 30°S close to zero. All acceptable model solutions show a dominance of northward flow of Antarctic Intermediate Water (AAIW) over warmer, upper layer waters, and all model solutions show net heat gain of the ocean from the atmosphere in the South Atlantic. The model results suggest that the upper-layer, northward flowing waters compensating the export of North Atlantic Deep Water (NADW) mainly consist of intermediate waters which enter through Drake Passage and which are modified and gradually warmed within the Atlantic. Direct, net inflow of large amounts of warm water from the Indian Ocean is not found in the model solutions and obviously not required. Forcing the model to produce such inflows actually compromises the model temperature and salinity fields.

Introduction

In recent years the South Atlantic has received increased attention and various research programs have been carried out to study the physical, geochemical and biological processes in this important part of the world ocean. The South Atlantic is unique because of its geographical location linking the Pacific, Indian and Atlantic Oceans. Various major water masses enter the South Atlantic. These water masses interact within the South Atlantic and are ultimately exported again with modified characteristics. Deepwater formed in the North Atlantic (NADW) passes through the South Atlantic and is exported to the Indian and Pacific oceans. This export of NADW must be compensated by northward flows of upper layer (warm surface and/or colder intermediate) waters and (Antarctic) bottom

From WEFER G, BERGER WH, SIEDLER G, WEBB DJ (eds), 1996, *The South Atlantic: Present and Past Circulation*. Springer-Verlag Berlin Heidelberg, pp 305-323

water in the South Atlantic. Because of the required northward upper layer flow it is generally believed that the South Atlantic transports heat northward, contrary to the general poleward heat transport in the other oceans (Bennett, 1978; Hastenrath, 1982).

Different and controversial pictures have emerged from numerous investigations on the origin, depth distribution and associated heat transport of the upper layer northward flow in the South Atlantic. Based on an upper layer heat budget calculation and using the relatively large heat flux estimate of Hastenrath (1982) at 30°S in the South Atlantic (0.69 PW to the north) Gordon (1986) concludes that the northward return flow in the South Atlantic occurs mainly in the warm thermocline layer and because no warm water is entering through Drake Passage is derived primarily from Indian Ocean Central Water (IOCW) entering the South Atlantic by a branch of the Agulhas Current that does not complete the retroflection and/or by warm-core eddies shed by the Agulhas in the retroflection region (warm water route). Because of the relatively low temperatures of the circumpolar waters flowing into the South Atlantic from the South Pacific Gordon (1986) estimates their contribution to the northward flow to be less than 25% of the Indian Ocean inflow.

The dominance of the warm surface water to the northward flow in the South Atlantic as proposed by Gordon (1986) has been questioned by Rintoul (1991) who uses hydrographic data from five non-synoptic sections in the South Atlantic and derives mass and heat transports by inverse calculations. He finds a substantial net inflow of upper IOCW (σ_0=26.80) to be incompatible with the hydrographic data. Contrary to Gordon (1986), Rintoul suggests that the northward flow in the South Atlantic is mainly derived from waters entering through Drake Passage (cold water route) and is equally split between the surface layers, and the intermediate and bottom waters. Rintoul (1991) estimates a meridional heat transport at 32°S of 0.25±0.12 PW, a value that is considerably smaller than Hastenrath's (1982) result. In a subsequent paper Gordon et al. (1992) use hydrographic and chlorofluoromethane (CFM) data from the southeast Atlantic and arrive at a circulation pattern that is different from the Gordon (1986) and Rintoul (1991) pictures. The northward flow in the South Atlantic now is composed of a large component of intermediate water entering through Drake Passage and partly flows eastward into the Indian Ocean before returning to the Atlantic. In addition to the intermediate water inflow the Gordon et al. (1992) scheme shows a contribution of about 10 Sv of water warmer than 9°C from the Indian Ocean.

In the present study the historical database of temperature and salinity measurements in the Atlantic is exploited, and the mean circulation in the South Atlantic obtained by driving a steady model towards the observations (using techniques from non-linear optimization theory) is investigated and discussed. Emphasis is on meridional mass and heat transports and the controversy on the origin and composition of the upper layer transport in the South Atlantic is addressed. Results from experiments with widely different values of meridional heat fluxes are presented and consistency of the various solutions with the data is investigated.

The Model

Fig. 1a shows the map of hydrographic stations used in the present study. The data collection contains more than 40,000 stations and has been obtained by merging individual datasets from J. Reid, W. Nowlin (personal communication), Fukumori, et al. (1991), the Southern Ocean Atlas of Gordon et al. (1986), and data from the U.S. NODC archive. All stations contain temperature and salinity data from the surface to the bottom. In general, data coverage is satisfactory, but in the South Atlantic data-gaps are evident some of which will be filled by the World Ocean Circulation Experiment (WOCE 1988) in the near future. The temporal distribution of the data in the South Atlantic is displayed in Figs. 1b to 1e and shows that the hydrographic data are mainly from the period 1950 to 1990 but that older data like, for instance, the Meteor and Discovery expeditions during the 1920's and 1930's (Wüst 1935; Deacon 1933) are included in the dataset as well (Figs. 1b and 1d). For the region between 55°S and the Equator all seasons are well represented, with stations from southern hemisphere spring and summer dominating only slightly over the fall and winter seasons (Fig. 1c). Southward of 55°S the

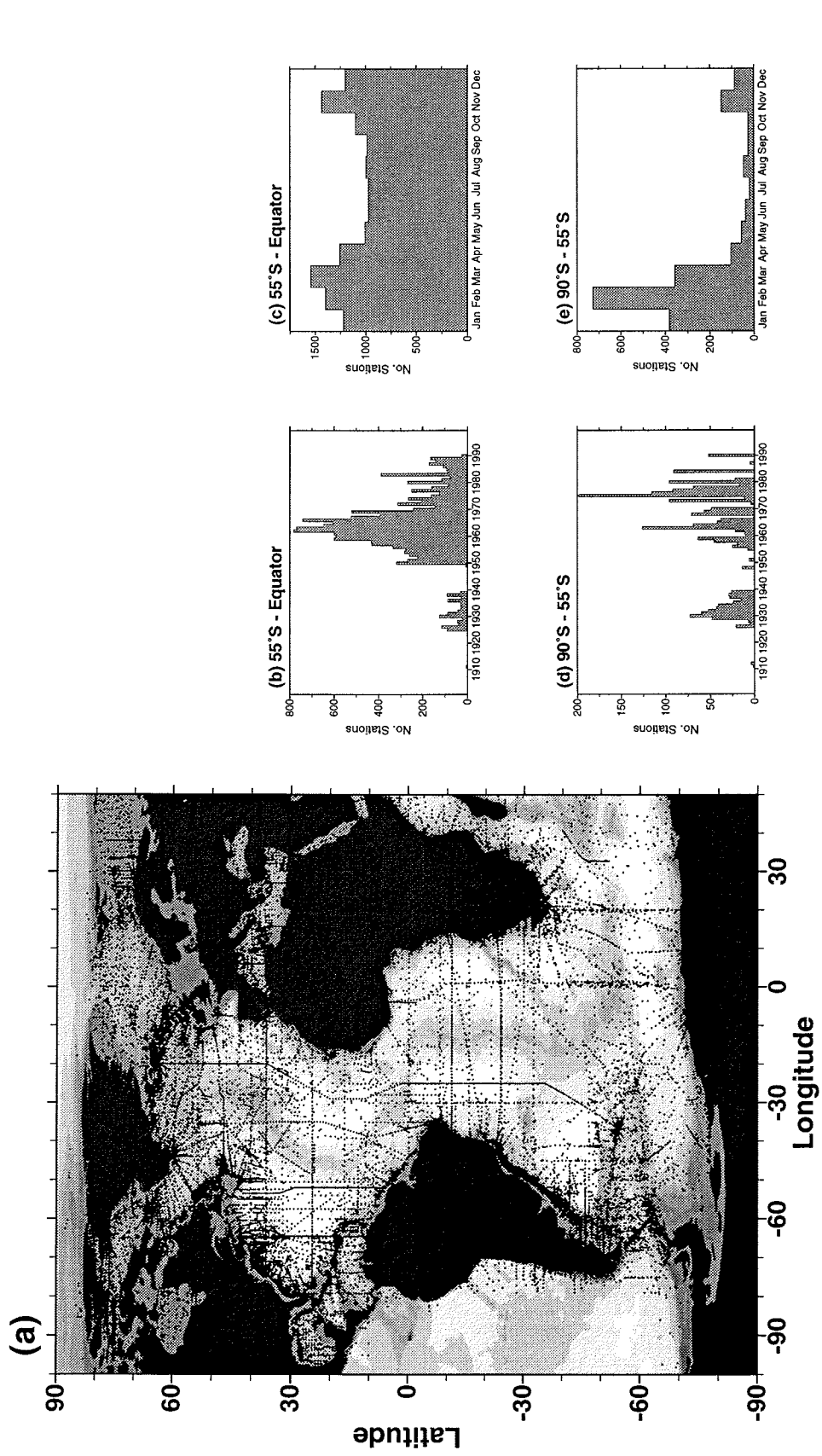

Fig. 1. Map of hydrographic stations used in this study (a) and temporal distribution of stations in the South Atlantic between 55°S and the Equator (b, c) and south of 55°S (d, e). In (a) bottom topography is indicated by gray-shading.

data are predominantly from the summer season (Fig. 1e). Overall, the available data appear to provide a good description of the hydrographic distributions during the last 60 years and can be considered a sound basis for an investigation of the long-term mean circulation and transport rates in the Atlantic as attempted here.

The tool used to extract information from the hydrographic data is a higher resolution version of the model described in Schlitzer (1993a) and Schlitzer (1993b). These papers contain a detailed description of model setup and model strategy and here only an overview of the general concept is given. The model domain encompasses the entire Atlantic including Weddell Sea, the Nordic Seas and the Arctic Ocean. Open ocean boundaries in Drake Passage, between South Africa and the Antarctic continent at 40°W and in Gibraltar and Bering Straits connect the model with the rest of the world ocean and allow exchange-flows with the Pacific, the Indian Ocean and with the Mediterranean. Horizontal model resolution is non-uniform ranging from 1x0.75° in areas with narrow currents (Gulf Stream, Agulhas, Antarctic Circumpolar Current (ACC) in Drake Passage, overflow region in the North Atlantic, western boundary currents) to 4x3° in most regions of the ocean interior (Fig. 2). Vertical resolution also is non-uniform with layer thickness varying from 60 m at the ocean surface to 500 m at 5000 m depth. The model has realistic topography based on the 5'x5' resolution US Navy bathy-metric data. Altogether the model consists of n_b=19776 control volumes (boxes). Neighboring boxes are connected via horizontal and vertical advective and diffusive fluxes, the respective velocities and mixing coefficients being defined in the center of the interfaces between the boxes.

For a given set of horizontal velocities u, v, air-sea heat fluxes Q and mixing coefficients K_h, K_v (u, v, Q and K_h, K_v comprise the independent parameters of the model) as well as boundary values for temperature and salinity at the open ocean boundaries taken from the data, the steady-state budget equations for mass, heat and salt are formulated for

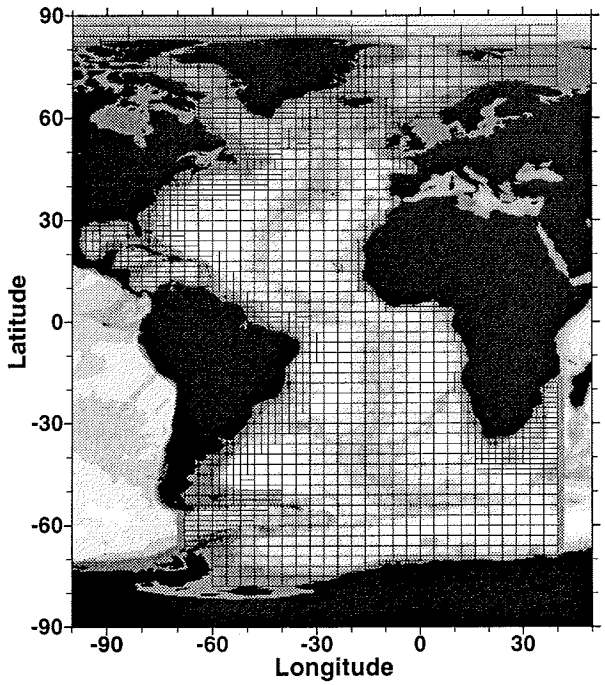

Fig. 2. Map of horizontal model grid. Open ocean boundaries are indicated by gray-shaded bars.

each box and the resulting sets of linear equations are solved for the vertical velocities w and the (steady-state) model potential temperatures θ_m and salinities s_m ("forward step"). Mass, heat and salt conservation is exact. Up to this point the model is similar to traditional box models (Broecker et al. 1960; Oeschger et al. 1974; Sarmiento 1983) even though the present model has a much higher resolution and a much larger number of boxes compared to the older box models.

The new feature of the Schlitzer (1993a; 1993b) concept comes into play when the quality of the current model state $p=[u, v, Q, K_h, K_v]$ is evaluated and model temperatures and salinities are compared with observations θ_d and s_d. For this, a cost function F is defined which, among other contributions, (see Schlitzer (1993a; 1993b) for a full list of terms and see Table 1 for an overview of a priori volume fluxes enforced using cost function terms) accumulates normalized, squared model-data misfits for temperature and salinity. A large value of F indicates large model-data deviations whereas a small value of F is indicative for a close agreement between model simulation and observations. As with traditional box models the overall goal is to minimize F (thereby achieving optimal agreement between simulation and data) by finding new, modified sets of model parameters (here: u^*, v^*, Q^* and K^*_h, K^*_v) that lead to better new simulated model values of temperature θ^*_m and salinity s^*_m. Whereas this step traditionally had to be performed manually (a formidable task for a complicated model like the present one), here it is performed automatically as part of the model calculations ("adjoint step", see Gill et al., (1981), Le Dimet and Talagrand (1986), Thacker (1988), Schlitzer (1993a, 1993b)). During the adjoint model step the structure of the model-data misfits is taken into account and a new, better model state $p^*=[u, v, Q, K_h, K_v]$ is constructed automatically at a computational cost comparable with the cost of the "forward" step.

The improvement or optimization of the current model state is a gradual, iterative process. Each time a better set of model parameters p^* consisting of horizontal flows, mixing coefficients and surface heat fluxes is found, the corresponding simulated temperatures and salinities θ^*_m and s^*_m are calculated. Then, the new, smaller model-data misfits are analyzed and an even better model state is obtained. When the decrease of F or the magnitude of the parameter modifications during one iteration are smaller than prescribed bounds, it is assumed that the minimum of F has been reached and the computations stop. An overview of this iterative process is given in the itemized flow-chart below.

0. *Initialization*. The horizontal model velocities (u, v) are set to geostrophic velocities calculated from the hydrographic data of Fig. 1. Following suggestions from the literature the reference level is not constant over the model domain, but

Table 1: *A priori* volume transports enforced by cost function terms (soft constraints) for all model experiments. Small tolerances and large weights imply a close reproduction of the *a priori* transport values by the model whereas large tolerances and small weights allow larger deviations.

Description	Transport [Sv]	Tolerance [Sv]	Weight
Bering Straits inflow into Arctic Ocean	1.0	0.1	10^5
Upper layer (0-500 m) inflow into Mediterranean	3.0	0.2	10^4
Net inflow into Mediterranean	0.04	0.01	10^6
Florida Current	30.0	1.0	50.
Drake Passage through-flow	130.0	2.0	10.

rises from about 3500 m at 60°S to about 1000 m at 50°N. Note that Ekman velocities based on winds from Trenberth et al. (1989) are added in the top two model layers. Air-sea heat fluxes Q (Oberhuber 1988) and mixing coefficients K_h and K_v (Olbers et al. (1985) and Olbers and Wenzel (1989)) are taken from the literature.

1. *Forward model run.* The independent parameters (u, v, Q, K_h, K_v) together with exact mass, heat and salt equations are used to calculate the dependent parameters (vertical velocities w, model temperatures θ_m, model salinities s_m).
2. *Adjoint model run.* The value of the cost function F and the gradient of F with respect to the independent parameters are calculated applying the adjoint method ("method of Lagrange multipliers") as an efficient means for obtaining gradients (see Gill et al. 1981; Thacker 1988 and Schlitzer 1993a; 1993b).
3. *Updating the independent parameters.* The gradient of F is passed to a descent algorithm (Gilbert and Lemaréchal 1989) to obtain a new, improved model state. In case a stopping criteria (e.g., sufficiently small decrease in F or sufficiently small modifications of the independent parameters) is satisfied the calculations terminate. Otherwise a new iteration is started at step 1.

It is important to note that in addition to the requirement to correctly reproduce the observed hydrographic fields the model velocities are required to approximately preserve the vertical velocity shear obtained by geostrophic calculations. The model may shift the velocity profile at a given location by a constant offset (the initially unknown reference velocity) without penalty, however, modifications to the shape of the velocity profiles lead to contributions to the cost function F. In this way, minimization of F forces the model velocity profiles to remain close to the geostrophic profiles and information in the hydrographic data on the oceanic pressure field are exploited by the model.

Model Results

In the following, results from three model experiments are presented and discussed. For experiment A only standard terms in the cost function F are employed (see Schlitzer (1993a; 1993b) for a full list of terms), whereas for experiments B and C constraints that force the zonally integrated meridional heat transport at various latitudes in the Atlantic to prescribed, a priori values are added (see Table 2). The prescribed meridional heat fluxes correspond to averages of literature values for experiment B but are close to maximal published values for case C. These experiments are carried out to investigate the sensitivity of the model and to determine the range of flow fields and transport rates for which satisfactory simulations of temperature and salinity can be obtained.

Cost Function

A summary of values of the total cost function F and individual terms for the three model experiments is shown in Table 3. Entries for experiment B are absolute values whereas entries for experiments A and C are normalized to case B (standard case) for easy comparison. It is found that experiments A (no heat transport constraints) and B ("average" meridional heat fluxes) lead to about the same final cost function value but that experiment C ("high" meridional heat fluxes) is significantly higher by a factor of 1.32. Inspection of the individual terms shows that for case A the distributions of air-sea freshwater and heat fluxes (terms 3 and 6) as well as the horizontal fields of vertical velocities w (term 4; calculated level by level) are smoother than for the standard case B. On the other hand, the agreement between model simulated property fields and observations (terms 7 to 14) is better for the standard case B compared with case A. The increased property misfits for experiment A are most pronounced for salinity and are largest in the South Atlantic south of 30°S (factor 1.28 compared to case B). Experiment C exhibits cost function terms significantly larger than those for the standard case B for both the smoothness terms and the terms measuring property misfits. For the entire model domain the systematic temperature deviations (term 9) are a factor of 1.45 larger compared with case B and systematic salinity deviations are a factor of 1.29 higher. Note that for all experiments A, B and C the deviations of the vertical velocity shear in the model from the geostrophic shear are

Table 2: *A priori* values for meridional heat transports [PW] at different latitudes for experiments B and C. The *a priori* values are enforced in the model by additional cost function terms (soft constraints).

Latitude	Experiment B	Experiment C
51°N	0.35	0.40
39°N	0.7	0.80
27°N	1.0	1.20
15°N	0.95	1.20
6°N	0.8	1.10
6°S	0.5	0.90
18°S	0.4	0.75
30°S	0.3	0.60

Table 3: Weight factors and values of total cost function and individual terms normalized to values of standard case B for different numerical experiments. Terms denoted "boxwise comparison" penalize property misfits box by box whereas for terms denoted "neighborhood" the mean misfit for a neighborhood of a box is calculated and this mean misfit is penalized. The latter terms are sensitive to systematic temperature and salinity deviations. See text for description of experiments and further comments on various cost function terms.

	Term	Weight	B	A	C
Σ	Total	–	$3.83 \cdot 10^{5}$	1.00	1.32
1:	Velocity shear	$1 \cdot 10^{-12}$	$9.12 \cdot 10^{-4}$	0.96	1.02
2:	E-P dat	2	$1.81 \cdot 10^{4}$	0.61	1.21
3:	E-P smoothness	$1 \cdot 10^{-1}$	$2.85 \cdot 10^{3}$	0.77	1.09
4:	w smoothness	1	$3.17 \cdot 10^{4}$	0.88	1.20
5:	Q data	5	$1.27 \cdot 10^{4}$	0.56	1.10
6:	Q smoothness	0.2	$2.10 \cdot 10^{4}$	0.75	1.15
7:	θ boxwise comparison	0.1	$6.96 \cdot 10^{4}$	1.10	1.31
8:	s boxwise comparison	0.1	$5.53 \cdot 10^{4}$	1.12	1.25
9:	θ neighborhood	0.01	$8.34 \cdot 10^{4}$	1.02	1.45
10:	s neighborhood	0.01	$6.73 \cdot 10^{4}$	1.23	1.29
11:	θ boxwise comparison $<30°S$	–	$1.96 \cdot 10^{4}$	1.14	1.27
12:	s boxwise comparison $<30°S$	–	$1.68 \cdot 10^{4}$	1.15	1.21
13:	θ neighborhood $<30°S$	–	$2.60 \cdot 10^{4}$	1.18	1.35
14:	s neighborhood $<30°S$	–	$2.36 \cdot 10^{4}$	1.28	1.25

small (see below) and of about the same size for all cases.

The terms in Table 3 representing systematic deviations between model temperatures or salinities and data for the whole model domain and for the region south of 30°S (items 9, 10, 13 and 14) are displayed in Fig. 3 versus the meridional heat flux at 30°S in the South Atlantic for each of the experiments. Also shown is a parabola fit through these points. Note that experiment A (no heat transport constraints) produces a poleward heat transport of -0.56 PW whereas experiments B and C closely match the prescribed values of +0.3 PW (B) and +0.6 PW (C), respectively. The parabola fit suggests that optimal agreement between model simulated and observed temperatures and salinity is achieved for a meridional heat flux in the South Atlantic at 30°S close to zero. The shape of the parabola indicates that near-optimal temperature and salinity simulations can be obtained for a wide range of model solutions. Based on a close inspection and analysis of model-data temperature and salinity differences for the three experiments a range of acceptable meridional heat transports at 30°S between about -0.5 PW and +0.4 PW is found. Experiment C is rejected mainly because of relatively large systematic temperature deviations. In the upper 400 m of the South Atlantic between 38°S and the equator experiment C is about 1°C too warm whereas in case B mean model temperatures agree with observations within 0.15°C.

Property Fields

As examples of model property fields, the salinity distributions of the standard case B in 200 m depth and along a meridional section at 30°W are displayed in Fig. 4 together with the corresponding distributions for the data. Figs. 4a and 4b show that the model correctly simulates the large-scale fea-

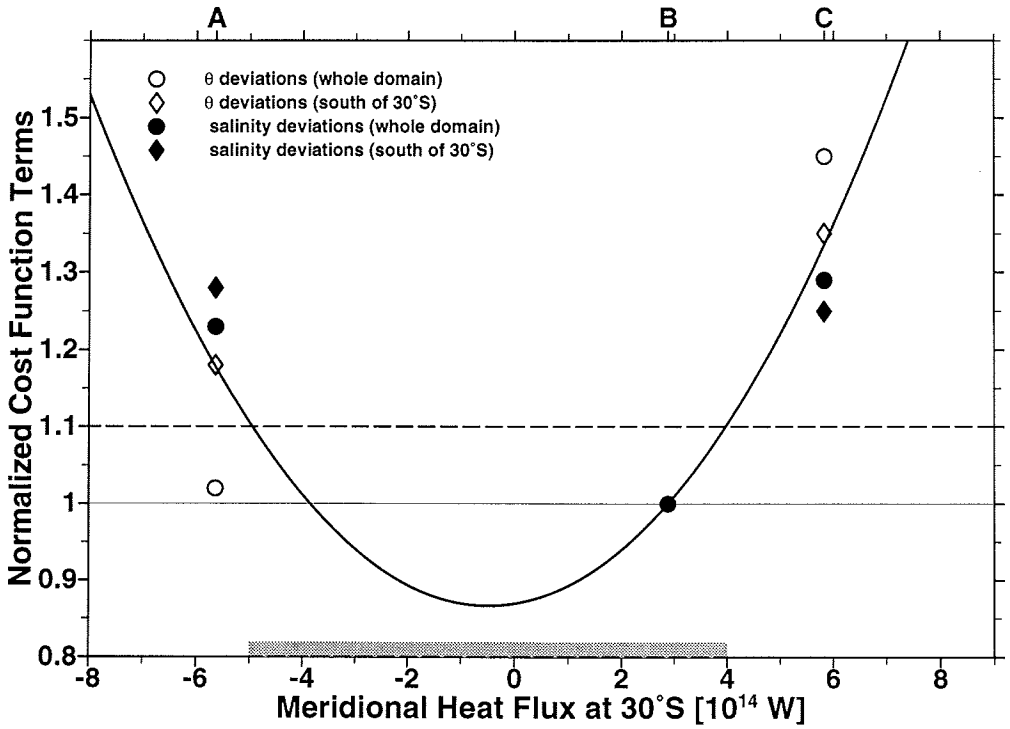

Fig. 3. Values of cost-function terms measuring temperature and salinity misfits of the model for different experiments (normalized to the standard case B) versus meridional heat transport across 30°S. The range of acceptable heat transports is indicated by a gray-shaded bar.

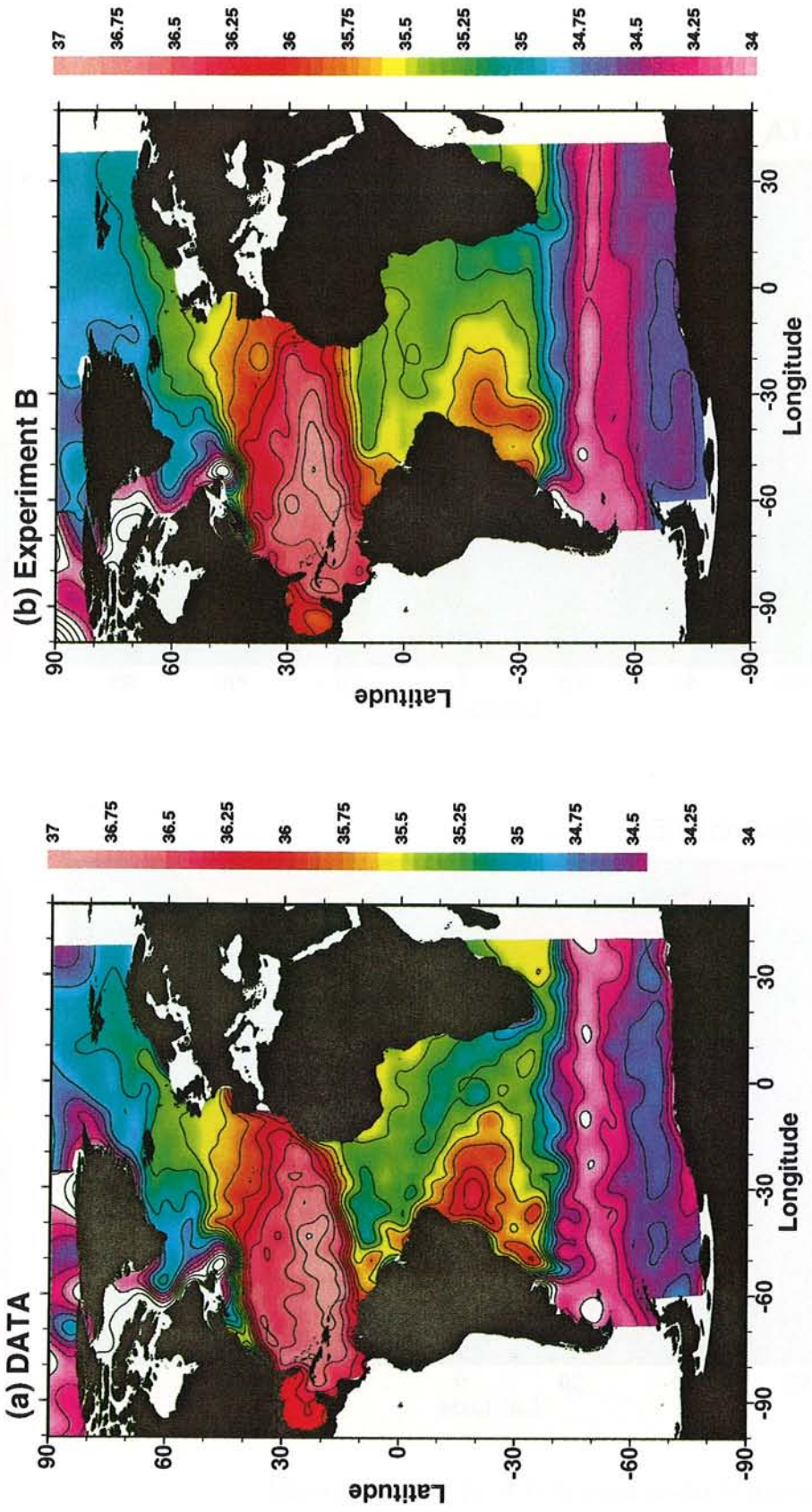

Fig. 4. Distribution of salinity at 200 m depth (a) data and (b) model (standard run B).

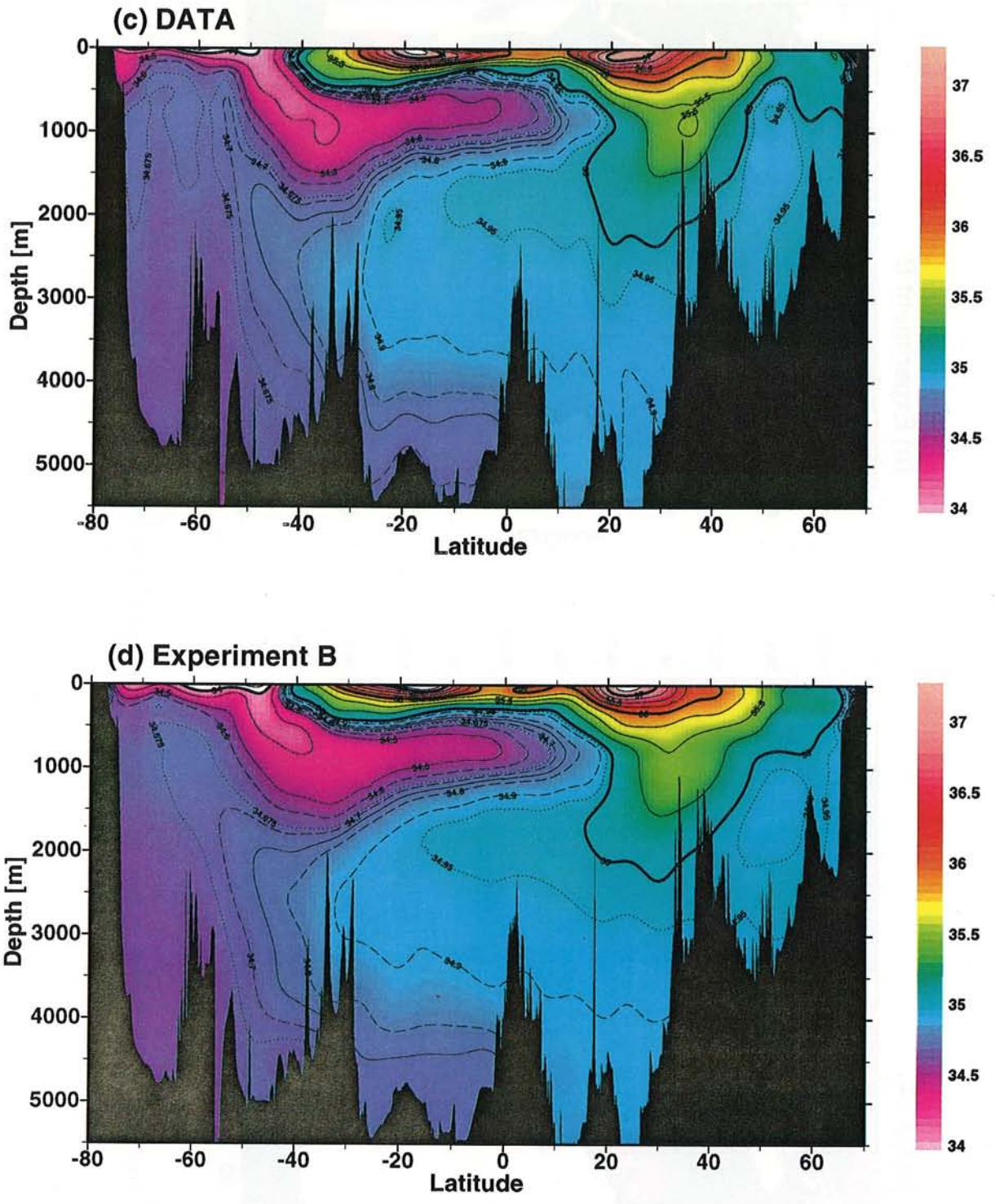

Fig. 4. Meridional section of salinity along at 30°W (c) data and (d) model.

tures in the salinity field in 200 m depth and that it reproduces the observed data values ranging from about 37 ppm in the center of the subtropical salinity maximum at 15°N to about 34 ppm in the salinity minimum along a zonal band at 50°S very closely. Even details like the salinity variations in the North Atlantic are modelled realistically. The meridional sections in Figs. 4c and 4d show that the model also produces the correct vertical layering and meridional extent of the major water masses in the Atlantic. Notably, features like the subtropical salinity maxima (the North Atlantic salinity maximum reaching deeper than South Atlantic maximum), the effect of the Mediterranean outflow in about 1200 m depth at 30°N, the subduction and spreading of low-saline Antarctic Intermediate Water (AAIW) in about 800 m depth in the South Atlantic, the southward reaching tongue of higher saline North Atlantic Deep Water (NADW) between about 1500 and 3500 m depth and the layer of lower salinity Antarctic Bottom Water (AABW) spreading northward are all correctly reproduced. Comparison of position and shape of the salinity isolines reveals a close quantitative agreement between model values and data.

Horizontal Flows

Fig. 5 shows geostrophic velocity profiles at seven locations in the South Atlantic together with the final velocities of the standard case B (note that the geostrophic flows are used to initialize the model velocities; see above). It is found that the vertical velocity shear of the final model flows remains close to geostrophic shear, and the modifications applied by the model are generally smaller than the temporal change of geostrophic velocity shear obtained from repeated observations. Most profiles show only small velocity offsets compared with geostrophic flows indicating that the selection of upward sloping reference depths with latitude between about 3000 and 2000 m in the South Atlantic (for exact reference depths see the zero-crossings of geostrophic profiles in Fig. 5) is appropriate. Exceptions are profile (c) in the eastern Cape Basin where velocities are shifted by about -0.4 cm s^{-1} in the final solution and now provide southward flow of NADW and profile (d) in the ACC east of Drake Passage where velocities are increased by about +1 cm s^{-1} and now are eastward at all depths. In areas where currents are narrower than the grid size of the model (e.g., profile (g) in the westward flowing, coastal branch of the Agulhas) the averaging of original hydrographic data, in general, leads to an underestimation of actual flow velocities (Olbers et al. 1985; Schlitzer 1993a; 1993b), and velocity modifications of the model in these regions are relatively large mainly because of mass conservation requirements.

Final, optimal model flows for the standard case B in 200 and 800 m depth in the South Atlantic are shown in Fig. 6. Dominant features in the shallow velocity field (Fig. 6a) are the eastward flowing Antarctic Circumpolar Current (ACC) and the Agulhas Current. In Drake Passage the ACC reaches speeds of up to 32 cm s^{-1} (average: about 20 cm s^{-1}) whereas in the South Atlantic (after turning northward and broadening) average velocities are decreasing to about 10 cm s^{-1}. Along the Argentine coast the Falkland/Malvinas Current flows northward and encounters subtropical waters that are transported southward with the Brazil Current in the Confluence region at about 40°S. The Brazil Current feeds the South Atlantic Current which flows eastward along about 40°S. Part of the South Atlantic Current folds into the Benguela Current and is transported north-westward with the South Equatorial Current. North of the triangular-shaped (anti-cyclonic) subtropical gyre consisting of Brazil Current, South Atlantic Current, Benguela Current and the southern branch of the South Equatorial Current, a cyclonic cell is found formed by the northern branch of the South Equatorial Current, the eastward flowing South Equatorial Counter Current and southward flows in the eastern Angola Basin. All the model flows found at 200 m depth (including the cyclonic Weddell Gyre) are in agreement with the general flow patterns of Reid (1989) and Peterson and Stramma (1991).

Model velocities in 800 m depth (largely representative of the circulation of AAIW in the South Atlantic) (Fig. 6b) are smaller than the surface flows (about 50%) but exhibit a similar spatial structure. As in Fig. 6a, highest velocities at this deeper level are observed in the ACC and Agulhas Current region. To the north of the ACC, centered

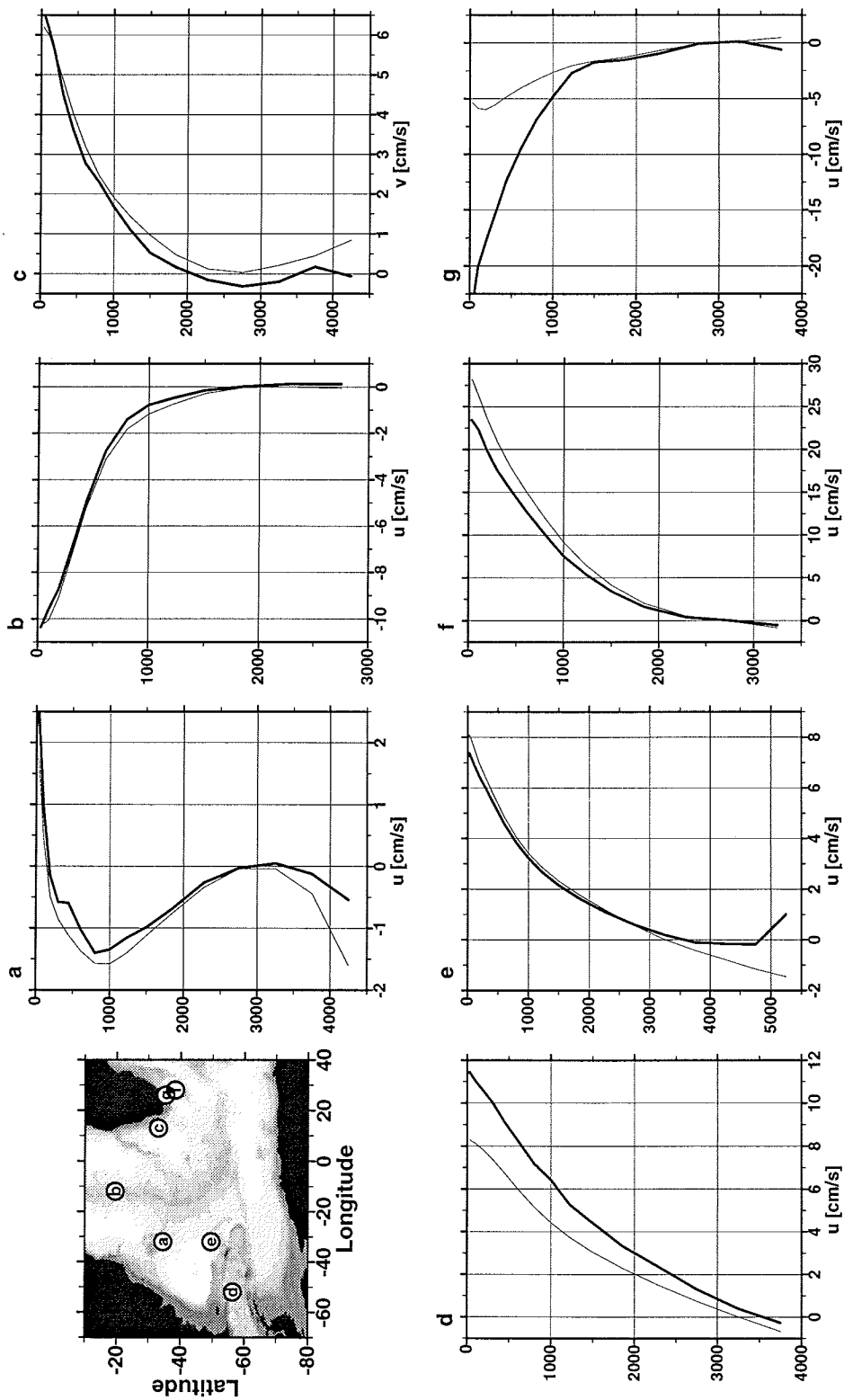

Fig. 5. Profiles of zonal (u) and meridional (v) velocities from geostrophic calculations (thin lines) and from standard-run B model flows (thick lines). Locations of individual profiles are indicated in the map. Note that the reference level of the initial geostrophic calculations is increasing with latitude (ca. 3500 m at 60°S and ca. 1000 m at 50°N).

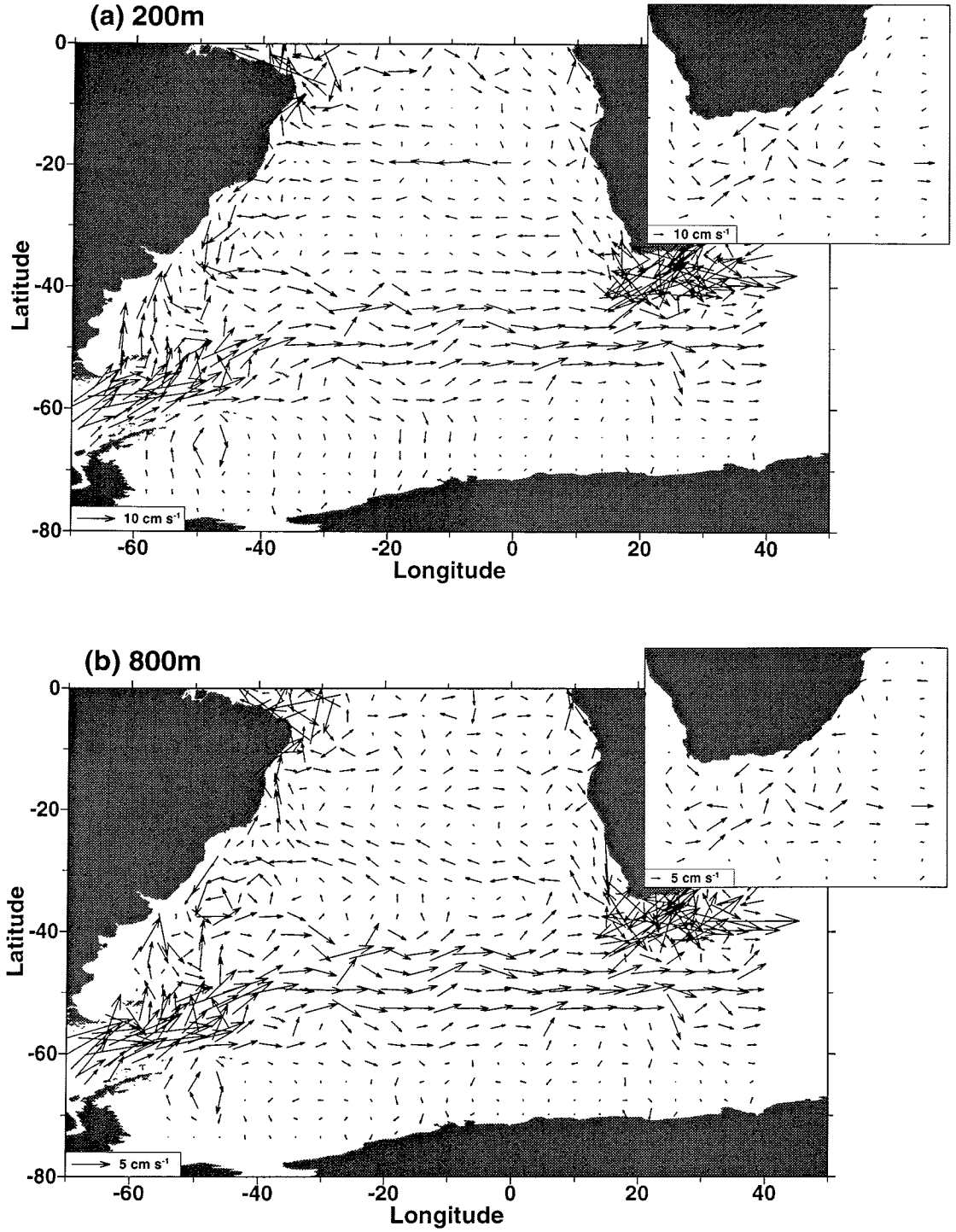

Fig. 6. Horizontal model flows of the standard-case B (a) in 200 m depth and (b) in 800 m depth. Arrows are vector averages of nearby zonal and meridional flow velocities.

at about 37°S, there is an almost rectangular, anticyclonic cell stretching across the entire South Atlantic. This cell consists of southward flow along the Brazilian coast, eastward flow along its southern boundary at about 44°S, northward flow near the African coast and westward flows at the northern boundary of the cell at about 30°S. Typical flow velocities are between 2 and 4 cm s^{-1}. A fraction of the water reaching the Brazilian coast near 24°S from the east is diverted northward. This water, in turn, partly continues into the North Atlantic as a western boundary current and partly turns eastward at about 13°S before flowing southward along the African coast. The circulation at 800 m depth in the South Atlantic north of about 45°S thus appears to be dominated by two, zonally stretched-out cells that are divided by relatively strong, almost zonal flows at about 30°S. In addition to temperature and salinity (see above), this flow pattern is consistent with the distributions of oxygen and chlorofluoromethane CFM-11 in the South Atlantic (see Figs. 4 and 11 of Warner and Weiss 1992). These distributions show a pool of newly ventilated intermediate water with high oxygen and CFM-11 concentrations south of 30°S and relatively "old" water with low oxygen and CFM-11 to the north. The model flows at 800 m depth also are in good agreement with the flow pattern of Reid (1989).

Integrated Transports

Integrated volume transports calculated for four isopycnal layers are presented in Fig. 7 for the standard experiment B and for experiment A. As shown in Fig. 3, both experiments produce temperature and salinity model fields that are in close agreement with observations. Fig. 3 also shows that solutions B and A differ markedly with respect to the meridional transport of heat at 30°S in the South Atlantic. Whereas experiment B transports about 0.3 PW of heat to the north, experiment A exhibits a southward heat transport of about -0.5 PW. Cases A and B, thus represent two extreme scenarios (in terms of meridional heat transports) that are found to be consistent with historic hydrographic data and with the principle of geostrophy. The four isopycnal layers for which transport rates are given represent major water masses found in the South Atlantic (1: surface water warmer than about 8-10°C, 2: AAIW, 3: NADW, 4: AABW) and closely correspond to subdivisions of Rintoul (1991) and Gordon et al. (1992).

For the standard case B (Fig. 7a) the meridional cell in the Atlantic consists of a southward transport of NADW of about 18 Sv (increasing from 17.1 Sv at 30°N to 17.8 Sv at the equator and 18.7 Sv at 30°S) that is compensated by northward transports of warm water, Antarctic Intermediate Water (AAIW) and Antarctic Bottom Water (AABW). At 30°S the intermediate water contribution (11.9 Sv) clearly dominates over the AABW (4.2 Sv) and warm water (2.0 Sv) transports. To the north, bottom and intermediate water transports decrease whereas the transport of warm water increases and at 30°N the NADW export is balanced predominantly by northward flow of warm water. In the equatorial Atlantic between 21°S and 15°N a net upwelling rate in 360 m depth of 6.3 Sv is found (compared to 10.6 Sv at 60 m depth) which is consistent with the decreasing flow of intermediate water and the increasing flow of warm water. From the South Atlantic south of 30°S there is a net export of warm water into the Indian Ocean of 21.9 Sv. Overall, more warm water is leaving this region than is entering through Drake Passage (the term "warm water" for waters in Drake Passage is misleading; maximal temperatures in its northern part are about 7.5°C and only because of very low salinities densities are less than σ_0=26.8). Associated with the net conversion of colder waters into warm water is a mean heat gain of the South Atlantic between 30°S and 60°S of 17.5 W m^{-2}. Integrated over the whole model domain experiment B shows a mean heat gain from the atmosphere of 0.45 W m^{-2} and a total freshwater loss to the atmosphere of 0.17 Sv. This net freshwater loss is obviously required for salt conservation because the dominant inflows into the Atlantic (AAIW, AABW across 30°S and Bering Strait inflow) are lower in salinity than the out-flowing NADW.

Meridional volume transports for experiment A (Fig. 7b) differ significantly from the values of the standard case B. Overall, experiment A shows a weaker meridional overturning cell with only about 13.5 Sv of NADW flowing southward. The northward transport of AAIW (18 Sv) is considerably

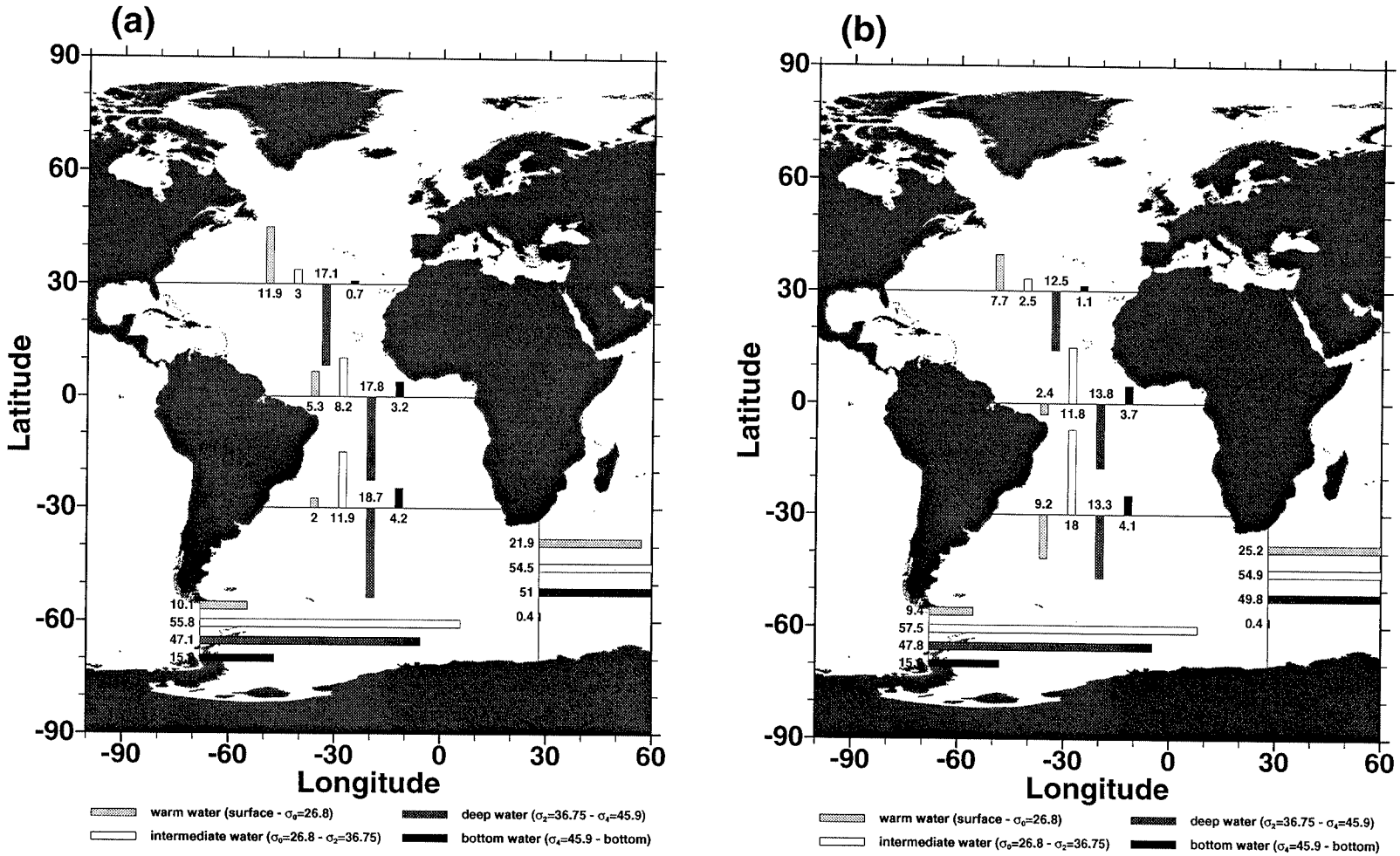

Fig. 7. Integrated volume transports [Sv] for four isopycnal layers representing major water masses in the Atlantic for (a) the standard case B and (b) for the case A exhibiting southward heat transport across 30°S. Note that any residual for the zonal sections in the Atlantic arises from inflow through Bering Strait and air-sea freshwater fluxes.

larger than for case B and the surface layer transport is now large and southward (-9.2 Sv). The northward flow of AABW is of about the same size as for the standard case B. Like case B, experiment A also exports more warm water from the South Atlantic than it receives, but because of the considerable inflow of warm water across 30°S the net warm water export is less than for the standard case B and consequently the net heat gain from the atmosphere of 4.8 W m^{-2} between 30°S and 60°S for experiment A is smaller than for experiment B. Integrated over the whole model domain the mean heat gain of experiment A is 5.7 W m-2 and the overall freshwater loss amounts to 0.27 Sv. These values are larger compared to case B because in solution A even more relatively cold, low salinity AAIW is transported northward across 30°S.

Fig. 8 shows the meridional heat transports of experiments B and A together with heat flux estimates from the literature. Whereas the standard case B with its relatively strong meridional overturning cell (18 Sv of southward flowing NADW) and moderate (2 Sv) contribution of warm water to the compensating northward transport exhibits heat transports that are about average when compared with literature values, experiment A deviates considerably from the other estimates, especially in the south and equatorial Atlantic. Owing to its large southward transport of warm, upper layer water (9.2 Sv at 30°S), meridional heat transports of experiment A are southward in the entire South Atlantic, in contradiction with the other values included in Fig. 8.

Conclusions and Discussion

The model calculations presented in this paper show that steady velocity fields (representing the long-term mean circulation in the Atlantic) that are consistent with geostrophic dynamics and successfully reproduce the observed distributions of temperature and salinity can be found. The set of solutions that satisfy these major model goals turns out to be relatively large including fields with widely differing meridional heat transports ranging from +0.4 PW to the north to -0.5 PW to the south. Associated with changes in meridional heat transports are changes in zonally integrated layer transports that can easily be obtained by small modifications of absolute flow velocities still remaining consistent with geostrophic calculations. In order to produce the seemingly large difference of warm water transports across 30°S between standard case B (+2 Sv) and experiment A (-9.2 Sv), typically, velocities in the ocean interior are changed by less than 0.1 cm s^{-1} and boundary current speeds are modified by at most 1.5 cm s^{-1}.

Model fields with a northward meridional heat transport at 30°S larger than 0.6 PW (experiment C) produce temperature and salinity simulations with significantly larger misfits compared with the optimal solutions and show temperature values in the upper layers of the South Atlantic that are systematically too warm by about 1°C. This systematic effect seems to be related to the relatively large inflow of warm Indian Ocean Central Water (IOCW) observed in these solutions. Acceptable IOCW inflows into the South Atlantic determined with model dye experiments (described elsewhere) range from 3.7 Sv (experiment A) to 6.5 Sv (standard case B). These values are much smaller than the estimate of Gordon (1986) (13.5 Sv) but are in good agreement with numbers based on chlorofluoromethane data (4 Sv, Gordon et al. (1992)) or the observations of Agulhas rings (5 Sv, Byrne et al. (1994); 6.2 Sv, Ballegooyen et al. (1994)).

The model results demonstrate that in order to produce a large northward transport of upper-layer, warm water in the North Atlantic compensating the southward export of NADW, an inflow of warm water of about equal size entering the South Atlantic from the Indian Ocean as proposed in the conveyor belt scheme of Gordon (1986) (warm water path) is not required and, when enforced, actually is found to be inconsistent with hydrographic data. Contrary to the warm water conveyor belt scheme and more in line with results of Rintoul (1991) and Boddem and Schlitzer (1995), both model solutions A and B show a dominance of AAIW to the upper layer northward transport in the South Atlantic (cold water path) and only small contributions of warm, surface water (as an extreme, experiment A even transports warm water to the south).

The apparent contrast between the warm and relatively salty upper layer waters in the North Atlantic and the low temperatures and salinities of

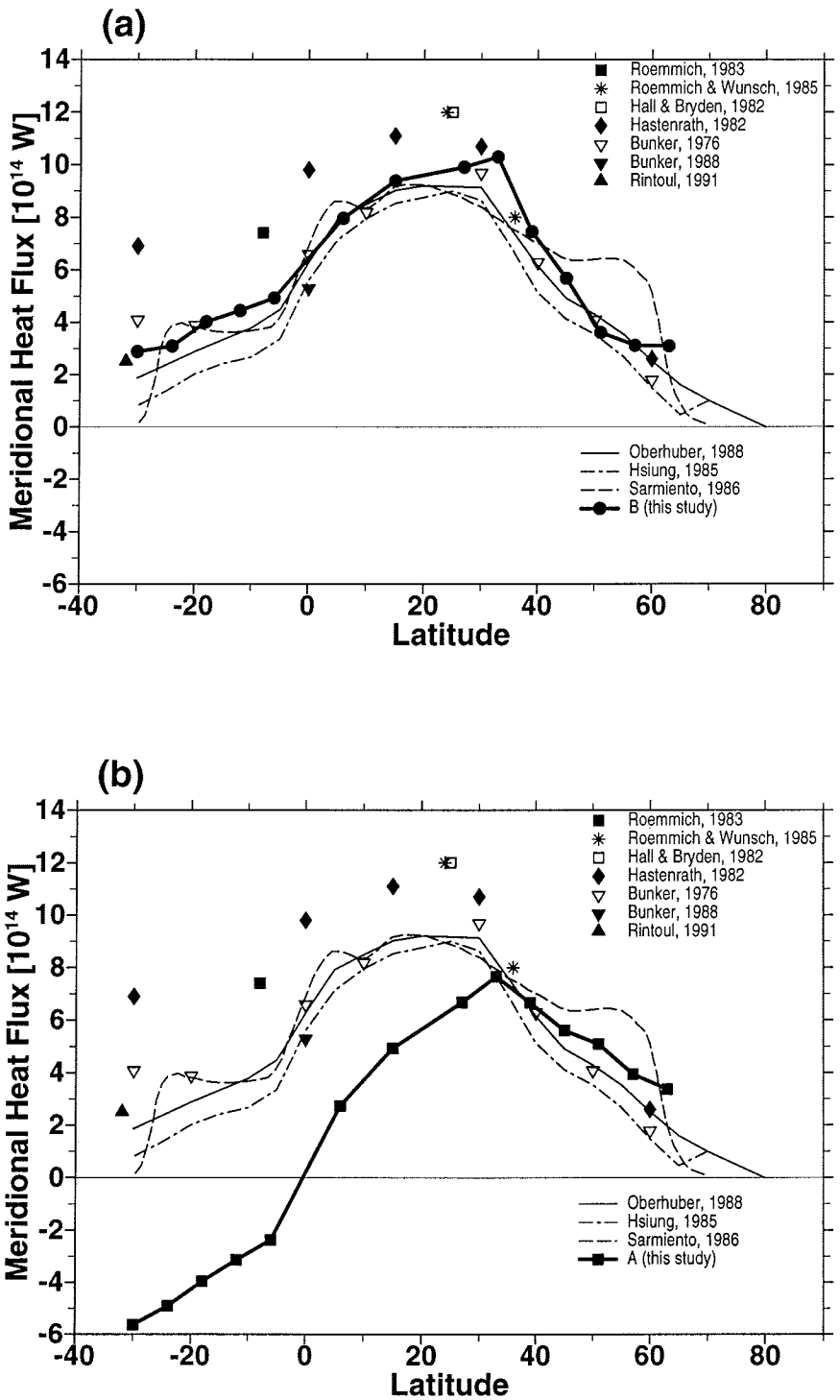

Fig. 8. Meridional heat transports versus latitude (a) for the standard case B and (b) for experiment A. Estimates from the literature are included for comparison.

its major source (according to this study) in the South Atlantic is resolved when taking into account air-sea freshwater and heat fluxes. The net air-sea freshwater fluxes for the whole model domain necessary to close the salt budget amount to +0.17 Sv excess evaporation for the standard case B and +0.27 Sv for experiment A with its very large northward flow of AAIW. These values are somewhat smaller than estimates from climatological calculations (+0.45 Sv; Baumgartner and Reichel (1975)) or hydrological, atmospheric models (+0.26 Sv; Broecker et al. (1990)) that also indicate net freshwater losses in the Atlantic. Common to all model solutions and also observed in other, independent heat-flux calculations (Bunker 1988) is a net heat gain of the South Atlantic between 30 and 60°S which is probably due to the about 10° of latitude equatorward shift of the relatively cold circumpolar surface waters east of Drake Passage. Mean heat gains in this area amount to between 17.5 W m^{-2} for the standard case B and 4.8 W m^{-2} for experiment A resulting in net warm water exports (in contrast to the net warm water inflow of the conveyor belt scheme) in both cases.

Fig. 3 showing the magnitude of temperature and salinity misfits of the three model experiments versus the meridional heat transport at 30°S is intriguing. Obviously, optimal agreement between hydrographic observations and model simulations is obtained for meridional heat fluxes at 30°S close to zero, but values up to 0.4 PW to the north and -0.5 PW to the south are seen to be consistent with data. Large heat fluxes like Hastenrath's (1982) value of 0.69 PW (used by Gordon (1986) to estimate the warm water inflow from the Indian Ocean into the South Atlantic), however, have to be rejected. The results of the present model calculations further increase the already large scatter of oceanic heat transport estimates (see for instance Fig. 8 and Peterson and Stramma (1991) their Fig. 28) by adding poleward heat transport values at 30°S to the existing list. Whether zero or even negative heat transports in the South Atlantic can also be found to be consistent with synoptic hydrographic section data remains to be investigated. The studies of Fu (1981) and Rintoul (1991) who use the same set of hydrographic data at 32°S and similar numerical techniques but arrive at considerably different heat transports at 32°S (0.77 and 0.23 PW, respectively) reveal the large error margins of oceanic heat flux values based on hydrographic data and suggest that reasonable reference velocities corresponding to zero or southward heat fluxes could be found. Sensitivity studies that explore upper and lower bounds of estimated heat flux values are obviously needed.

This is publication 1007 of the Alfred Wegener Institute for Polar and Marine Research and contribution 119 of the Sonderforschungsbereich 261 at Bremen University.

References

van Ballegooyen RC, Gründlingh ML, Lutjeharms JRE (1994) Eddy fluxes of heat and salt from the southwest Indian Ocean into the southeast Atlantic Ocean: a case study. J Geophys Res 99:14,053–14,070

Baumgartner A, Reichel E (1975)The World Water Balance. Oldenbourg–Verlag, Munich, Federal Republic of Germany

Bennett AF(1978) Poleward heat fluxes in southern hemisphere oceans. J Phys Oceanogr 8:785–798

Boddem J, Schlitzer R (1995) Interocean exchange and meridional mass and heat fluxes in the South Atlantic. J Geophys Res 100:15,821-15,834

Broecker WS, Gerard R, Ewing M, Heezen BC (1960) Natural radiocarbon in the Atlantic Ocean. J Geophys Res 65:2903–2931

Broecker, WS, Peng T-H, Jouzel J, Russel G (1990) The magnitude of global fresh-water transports of importance to ocean circulation. Clim Dyn 4:73–79

Bunker, AF (1988) Surface energy fluxes of the south Atlantic Ocean. Mon Weath Rev 116:809–823

Byrne DA, Gordon AL, Haxby WF (1994) Agulhas eddies: a synoptic view using Geosat ERM data. J Phys Oceanog (submitted)

Deacon GER (1933) A general account of the hydrology of the South Atlantic Ocean. Discovery Reports 7:171–238

Fu L-L (1981) The general circulation and meridional heat transport of the subtropical South Atlantic determined by inverse methods. J Phys Oceanogr 11:1171–1193

Fukumori I, Martel F, Wunsch C (1991) The hydrography of the North Atlantic in the early 1980s. An atlas. Prog Oceanog 27:1–110

Gilbert J Ch, Lemaréchal C (1989) Some numerical

experiments with variable-storage quasi-Newton algorithms. Mathematical Programming 45:407-435

Gill PE, Murray W, Wright MH (1981) Practical Optimization. Academic Press, London

Gordon AL, Weiss RF, Smethie WM, Warner MJ (1992) Thermocline and Intermediate Water Communication between the South Atlantic and Indian Oceans. J Geophys Res 97:7223–7240

Gordon AL (1986) Interocean exchange of thermocline water. J Geophys Res 91:5037–5046

Gordon AL, Molinelli EJ, Baker TN (1986) Southern Ocean Atlas. Amerind Publishing Co., New Dehli

Hastenrath S (1982) On meridional heat transports in the world ocean. J Phys Oceanog 12:922–927

Le Dimet F, Talagrand O (1986) Variational algorithms for analysis and assimilation of meteorological observations : theoretical aspects. Tellus 38:97–110

Oberhuber JM (1988) An atlas based on the COADS data set: the budgets of heat, buoyancy and turbulent kinetic energy at the surface of the global ocean. Technical Report 15, Max-Planck-Institut für Meteorologie, Hamburg

Oeschger H, Siegenthaler U, Schotterer U, Gugelmann A (1974) A box diffusion model to study the carbon dioxide exchange in nature. Tellus 27:168–192

Olbers D, Wenzel M, Willebrand J (1985) The inference of north Atlantic circulation patterns from climatological hydrographic data. Rev Geophys 23:313–356

Olbers D, Wenzel M (1989) Determining diffusivities from hydrographic data by inverse methods with applications to the Circumpolar Current. In: Oceanic Circulation Models: Combining Data and Dynamics. Kluwer Academic Publishers, Dordrecht, 95–139

Peterson RG, Stramma L (1991) Upper-level circulation in the South Atlantic ocean. Prog Oceanogr 26:1–73

Reid JL (1989) On the total geostrophic circulation of the South Atlantic Ocean: flow patterns, tracers, and transports. Prog Oceanogr 23:149–244

Rintoul SR (1991) South Atlantic interbasin exchange. J Geophys Res 96:2675–2692

Sarmiento JL (1983) A tritium box model of the north Atlantic thermocline. J Phys Oceanogr 13:1269–1274

Schlitzer R (1993a) Determining the mean, large-scale circulation of the Atlantic with the adjoint method. J Phys Oceanogr 23:1935–1952

Schlitzer R (1993b) An adjoint model for the determination of the mean oceanic circulation, air-sea fluxes and mixing coefficients. Habilitation Thesis, University Bremen

Stramma L, Peterson RJ (1990) The South Atlantic Current. J Phys Oceanog 20(6):846–859

Thacker WC (1988) Three lectures on fitting numerical models to observations. Technical Report GKSS 87/E/65, GKSS Forschungszentrum, Geesthacht

Trenberth KE, Olsen JG, Large WG (1989) A global ocean wind stress climatology based on ECMWF analyses. Technical Report NCAR/TN-338+STR, National Center for Atmospheric Research, Boulder

Warner MJ, Weiss RF (1992) Chlorofluoromethanes in south Atlantic Antarctic Intermediate Water. Deep-Sea Res 39:2053–2075

WOCE (1988) World Ocean Circulation Experiment Implementation Plan. Vol I, World Meteorological Organization, Wormley, Report 242

Wunsch C (1984) An eclectic Atlantic Ocean circulation model. Part I: The Meridional Flux of Heat. J Phys Oceanog 14:1712–1733

Wüst G (1935) Schichtung und Zirkulation des Atlantischen Ozeans: Die Stratoshäre. Wiss. Ergeb. Dtsch. Atlantischen Exped. Forschungs- und Vermess. Meteor 1925-1927, 6(1st part, 2), p. 180 (English translation by the Al-Ahram Center for Scientific Translations, WJ Emery, 112, Amerind, New Delhi 1978)